Available online at www.sciencedirect.com

SciVerse ScienceDirect

Scripta Materialia 69 (2013) 413–416

Scripta MATERIALIA

www.elsevier.com/locate/scriptamat

The five-parameter grain boundary character distribution of nanocrystalline tungsten

Xuan Liu,[a] Dooho Choi,[a] Hossein Beladi,[b] Noel T. Nuhfer,[a] Gregory S. Rohrer,[a] and Katayun Barmak[c,*]

[a]*Department of Materials Science and Engineering, Carnegie Mellon University, 5000 Forbes Avenue, Pittsburgh, PA 15213, USA*

[b]*Institute for Frontier Materials, Deakin University, Geelong, VIC 3216, Australia*

[c]*Department of Applied Physics and Applied Mathematics, Columbia University, 500 W. 120th St., New York, NY 10027, USA*

Received 12 April 2013; revised 22 May 2013; accepted 29 May 2013
Available online 7 June 2013

Transmission electron microscopy has been used to collect high-resolution orientation maps from a tungsten thin film with a 100 nm average grain size. The orientation distribution of grain boundary planes at specific lattice misorientations is non-uniform and has characteristics similar to materials with larger grain sizes. A comparison of the populations of grain boundaries in tungsten with the same boundaries in a ferritic steel suggests that polycrystals with a body-centered cubic crystal structure have similar grain boundary character distributions.

Keywords: Grain boundaries; Nanocrystalline; Tungsten; Precession electron diffraction

The properties of materials, including electrical resistivity [1,2], mechanical response [3], corrosion resistance [4], and dielectric phenomena [5] are influenced by the types of grain boundaries within the material and how they are connected. Using established orientation mapping techniques [6], it has become possible to measure the relative areas of different types of grain boundaries over all five independent crystallographic parameters [7]. This quantity, known as the five-parameter grain boundary character distribution (GBCD), is usually parameterized in terms of the lattice misorientation and grain boundary plane orientation. Past measurements of the GBCD have been carried out exclusively using electron backscatter diffraction (EBSD) in a scanning election microscope (SEM). While the point-to-point resolution of EBSD can be in the range of a few tens of nanometers, depending on the electron source and sample [8,9], measurement of the GBCD requires that the shapes of the boundaries be characterized and, because of this, it has not been possible to accurately measure the GBCD of samples with average grain sizes much smaller than 1 micrometer in diameter. Because of this experimental limitation, it has not been possible to determine the extent to which the GBCDs of nanocrystalline materials differ from, or are similar to, the GBCDs of microcrystalline materials.

It has recently been demonstrated that orientation mapping is possible using a transmission electron microscope (TEM) [10–12]. In this technique, diffraction patterns are acquired while the electron beam is moved along a conical surface, reducing the dynamical diffraction effects and making the patterns easier to index. This technique increases the spatial resolution by a factor of 10 compared to SEM-based techniques, and was recently used to measure the distribution of grain boundary planes for Σ3 boundaries in Cu [13]. In the present paper, we describe the use of the same technique to measure the complete five-parameter grain boundary character distribution in a nanocrystalline, body-centered cubic (bcc) metal, tungsten. Even though the average grain size of the tungsten film was only 100 nm, the distribution of grain boundary planes at fixed misorientation was clearly revealed. The similarity of the distribution to that measured for microcrystalline iron suggests that materials with bcc crystal structures have

* Corresponding author. Tel.: +1 2128548267; e-mail: katayun.barmak@columbia.edu

1359-6462/$ - see front matter © 2013 Acta Materialia Inc. Published by Elsevier Ltd. All rights reserved.
http://dx.doi.org/10.1016/j.scriptamat.2013.05.046

correlated grain boundary character distributions and that, in this case, the GBCD of a nanocrystalline material is not significantly different from that of microcrystalline material with the same crystal structure.

The sample examined here was a 43 nm thick W film. The film was one in a series used to investigate the resistivity of thin W films. The W films were sputter deposited from a 99.95% pure W target onto oxidized Si wafers at room temperature. A subset of the films, including the film in the current study, was encapsulated in an underlayer and an overlayer of sputter-deposited silicon dioxide. The aim of this encapsulation was to provide identical top and bottom electron scattering surfaces, and to prevent film agglomeration during annealing [14]. Following deposition, the film was annealed at 850 °C for 2 h in an Ar–4% H_2 atmosphere to transform any remaining metastable beta W (A15) in the first 5–10 nm of the deposited film to alpha W (A2, bcc) [15]. No grain growth took place during annealing; therefore, the grain size of the annealed film was the same size as that of the as-deposited film, and was determined by the nucleation density of alpha W in beta W. Additional details of film preparation and characterization can be found in Ref. [15].

To prepare an electron-transparent region for TEM analysis, the sample was thinned from the back side, first removing most of the Si by mechanical polishing and then removing the remainder by acid etching. All of the orientation maps were recorded using an ASTAR™ (NanoMEGAS, Brussels, Belgium) system installed on a FEI Tecnai F20 TEM (FEI Corporation, Hillsboro, OR) with a field emission gun and an accelerating voltage of 200 kV. Diffraction patterns were recorded with a precession angle of 0.3°, and orientation maps (see Fig. 1) were recorded with a step size of 5 nm.

The orientation maps were analyzed using TSL OIM software (EDAX, Mahwah, NJ, USA) after adjusting for the reference frame difference between the ASTAR™ and TSL systems, as described in detail elsewhere [13,16]. In this case, a counterclockwise rotation of 207° was used to bring the diffraction pattern and image into coincidence. The orientation data was subjected to a clean-up procedure to eliminate unindexed and incorrectly indexed points, including points near grain boundaries due to the overlap of diffraction patterns from adjacent grains. First, the grain dilation filter was used with a minimum grain size of 15 pixels and a tolerance angle of 5°. Next, a single, averaged orientation was assigned to all of the pixels within a grain, assuming that all adjacent pixels with misorientations less than 5° belonged to the same grain. Next, the pseudosymmetry clean-up was used to remove false boundaries that are created within single grains when patterns can be indexed in multiple orientations related by simple symmetry operations. Here, false 60° ⟨1 1 1⟩ boundaries were removed with a tolerance of 2° and false 180° boundaries were removed with a tolerance of 1°. These clean-up procedures change fewer than 6% of all of the orientation points in the maps. Grain boundary line segments were then extracted from the orientation maps using the reconstructed boundary segments feature. The reconstructed boundary segments deviated from the true boundary positions by no more than two pixels. The final set of observations consisted of ~57,000 grain boundary line segments extracted from 46 fields of view. A typical orientation map is shown in Figure 1a before clean-up, and in Figure 1b after clean-up, with the reconstructed grain boundary line segments superimposed. The GBCD was determined from the grain boundary line segments using a previously described stereological method of analysis [17] that has been applied to a wide range of polycrystals [18]. When the calculation of the GBCD was repeated under the assumption that all of the grain boundaries are perpendicular to the surface, no significant differences were found. The GBCD of a high-strength, low-alloy (HSLA) ferritic steel, used here for comparison, was collected using three-dimensional EBSD; the experiment is described in full in an earlier publication [19].

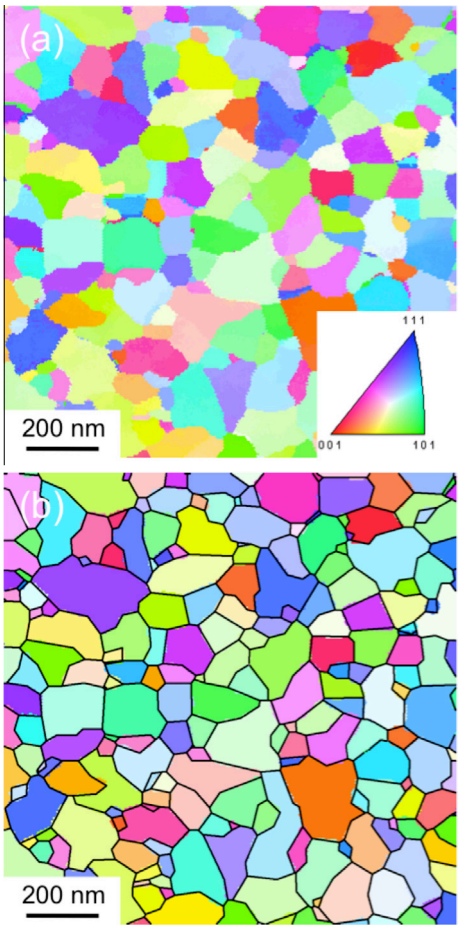

Figure 1. Representative orientation map of the W thin film. (a) The raw map before clean-up; (b) cleaned data with reconstructed grain boundary line segments (black lines) superimposed. The grains are colored by orientation according to the inset key.

The microstructure consisted of equiaxed grains. Based on the 10,000 grains in the orientation maps, the average grain size was 100 nm. This value is equal, within experimental error, to the previously reported value of 101 ± 6 nm obtained by the conical dark-field imaging using the ACT (automated crystallography in the transmission electron microscope) system [15]. Note that the average grain diameter is more than twice the film thickness, meaning that most of the grains span

the film thickness. With a step size of 5 nm, there are an average of 20 scan points per grain diameter, which is sufficient for accurately measuring the grain shapes. The sample showed no significant orientation texture and the distribution of disorientation angles (not shown) did not deviate significantly from a random distribution.

Grain boundary plane distributions at fixed misorientations had relatively modest anisotropies, comparable to other bcc materials [19,20]. Four grain boundary plane distributions are plotted on stereographic projections in Figure 2. Two of the highest peaks in the distribution occur at the Σ3 (60° around [1 1 1]) and Σ17b (60.9° around [2 1 2]) misorientations, shown in Fig. 2(a) and (b), respectively. At the Σ3 misorientation, there is a minimum at the (1 1 1) twist position and a continuously high population of grain boundaries along the zone of pure tilt grain boundaries perpendicular to (1 1 1). This preference for Σ3 tilt GBs is consistent with other bcc materials [19,20]. The small variations within this zone are not significant; the symmetric tilt boundaries at the $(\bar{1}\,1\,2)$, $(\bar{1}\,\bar{1}\,2)$ and $(1\,\bar{1}\,2)$ orientations and other asymmetric boundaries are preferred, and are occupied with approximately the same probability. In this case, it is interesting that the preference is not for a particular grain boundary orientation, but for any grain boundary in the [1 1 1] zone.

For the other three distributions illustrated in Figure 2, there is a clear preference for a single low index plane. For the Σ17b grain boundary, the peak is in the $(1\,\bar{1}\,0)$ and $(\bar{1}\,1\,0)$ positions. In this representation, this is a mixed boundary. However, a symmetrically equivalent representation of the Σ17b misorientation, outside the fundamental zone, is the boundary with a 93.6° rotation about $[\bar{1}\,1\,0]$; in that representation, this is a pure twist grain boundary [21]. In the cases of the low angle boundary (Σ1, 10°/[1 1 1]) and the Σ11 boundary (50.5°/[1 1 0]), the maxima also occur at the positions of the pure twist grain boundary, (1 1 1) and (1 1 0), respectively.

The GBCDs of two other metals with the bcc structure have been reported: an interstitial free steel [20] and an HSLA ferritic steel [19]. Simple visual comparisons of the distributions of grain boundary planes at specific misorientations show that there are similarities among these materials. To quantify these similarities, we compare the GBCDs of W and the HSLA steel in the following way. For W, we find all grain boundaries within a certain population interval, 0.1 multiples of a random distribution (MRD) wide, and average the populations. Next, we find the populations of the same grain boundaries (same five crystallographic parameters) in the ferritic steel, and determine the average. When the average populations of the same subset of boundaries are used as coordinates for each population interval, the plot in Figure 3 results. This analysis shows that there is a strong correlation between the two distributions. On average, grain boundaries that occur infrequently in W also occur infrequently in the ferritic steel and the most common boundaries in W are also common in the ferritic steel. It should be noted that this is an average correlation; for certain individual points in the five-parameter space, the correlation is not expected to be as strong.

The correlation between these two distributions is likely to be related to the grain boundary energy. It is well established that, for microstructures evolving by normal grain growth, there is an inverse correlation between the grain boundary population and the grain boundary energy [22,23] . Recently, simulations have been used to demonstrate that the grain boundary energies of different face-centered cubic (fcc) structured metals were strongly correlated [24] and that this leads to correlations in the GBCDs of fcc metals [25]. Assuming that a similar phenomenon occurs in bcc metals, this would account for the strong correlations between the GBCDs of W and the ferritic steel. It is important to note that the microstructure of the tungsten film was determined during deposition and was not created by grain growth. However, it is safe to assume that the grain boundary planes had the opportunity to achieve

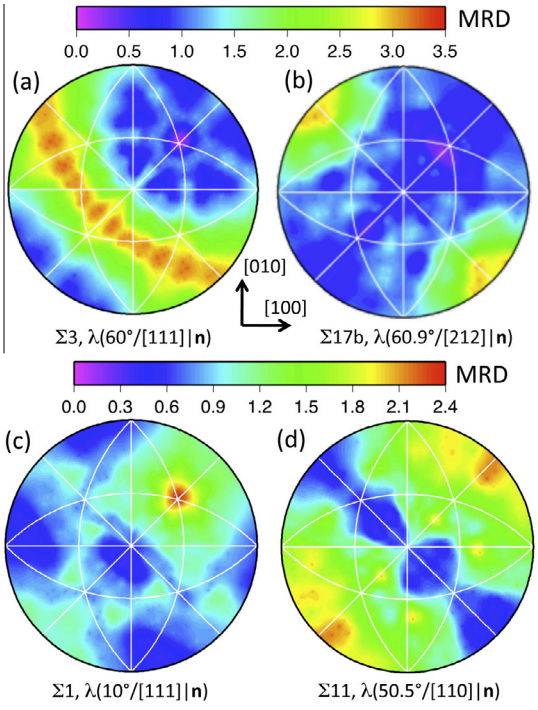

Figure 2. Grain boundary plane distributions at fixed misorientations: (a) Σ3, 60°/[1 1 1], (b) Σ17b 60.9°/[2 1 2], (c) Σ1, 10°/[1 1 1], (d) Σ11, 50.5°/[1 1 0]. The distributions are plotted in stereographic projection in units of MRD. The positive [1 0 0] direction is horizontal and to the right. The positive [0 1 0] direction is vertical and upward.

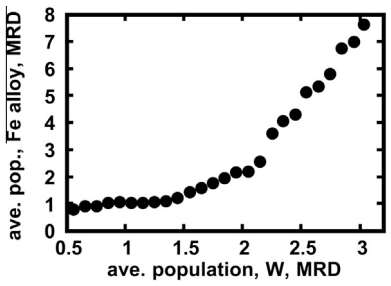

Figure 3. For all grain boundaries within a population interval of 0.1 MRD in W, the average populations of the same boundaries in a ferritic steel are plotted.

low energy orientations. If this were not the case, the microstructure would be similar to a Voronoi structure, and this is clearly not the case in Figure 1. The positioning of the grain boundary planes accounts for the non-uniform distributions at fixed misorientations. On the other hand, the absence of grain growth explains the absence of texture in the misorientation distribution. The stronger misorientation texture in the ferritic steel, which develops during grain growth and enhances the population of low energy boundaries, is the reason why the slope of the data in Figure 3 is greater than unity.

The suggestion that the grain boundary energies of Fe and W are correlated is supported by the fact that recent calculations of the energies of grain boundaries in bcc Fe appear to be inversely correlated to populations in nanocrystalline W. Two reports conclude that the Σ3, (2 1 1), symmetric tilt boundary has the lowest energy [26,27]. An experimental evaluation of the energies in a ferritic steel reached the same conclusion [19]. This grain boundary is among the Σ3 tilt boundaries that have the highest population in nanocrystalline W. Also, for the Σ3 grain boundary, Kim et al. [26] find the energy maximum at (1 1 1), where we find the population minimum. For the Σ9 grain boundary, the same authors find the energy minimum at (1 1 0) and the energy maxima along the zone of tilt boundaries perpendicular to [1 1 0]; this is consistent with the measurements reported for the ferritic steel [19]. While not shown here, the grain boundary plane distribution for Σ9 boundaries in tungsten is similar to the distribution shown in Figure 2(d), and the maxima and minima are inversely correlated to energies calculated by Kim et al. [26] for Fe.

In summary, the grain boundary character distribution of a nanocrystalline metal has been measured by a TEM orientation mapping technique. The GBCD of nanocrystalline W is not significantly different from bcc structured metals with larger grain sizes. In fact, the distribution is strongly correlated to that of a ferritic steel with an average grain size that is 10–100 times larger.

Financial support of the SRC, Task 1292.008, 2121.001 and 2323.001, and of the MRSEC program of the NSF under DMR-0520425 is gratefully acknowledged. G.S.R. acknowledges financial support from the ONR-MURI under Grant No. N00014-11-1-0678. The work at Deakin University was supported through grants provided by the Australian Research Council.

[1] B. Feldman, S. Park, M. Haverty, S. Shankar, S.T. Dunham, Phys. Status Solidi B 247 (2010) 1791–1796.
[2] L. Lu, Y.F. Shen, X.H. Chen, L.H. Qian, K. Lu, Science 304 (2004) 422–426.
[3] L.C. Lim, T. Watanabe, ScM 23 (1989) 489–494.
[4] S.A. Xia, B.X. Zhou, W.J. Chen, J. Mater. Sci. 43 (2008) 2990–3000.
[5] S.B. Lee, T.S. Key, Z. Liang, R.E. Garcia, S. Wang, X. Tricoche, G.S. Rohrer, Y. Saito, C. Ito, T. Tani, J. Eur. Ceram. Soc. 33 (2013) 313–326.
[6] B.L. Adams, S.I. Wright, K. Kunze, Metall. Mater. Trans. A 24 (1993) 819–831.
[7] G.S. Rohrer, D.M. Saylor, B. El Dasher, B.L. Adams, A.D. Rollett, P. Wynblatt, Z. Metallkd. 95 (2004) 197–214.
[8] F.J. Humphreys, J. Mater. Sci. 36 (2001) 3833–3854.
[9] S. Zaefferer, Ultramicroscopy 107 (2007) 254–266.
[10] E.F. Rauch, K. Barmak, K. Ganesh, P. Ferreira, A. Darbal, D. Choi, T. Sun, B. Yao, K. Coffey, S. Nicolopoulos, Microsc. Microanal. 17 (2011) 1086–1087.
[11] E.F. Rauch, L. Dupuy, Arch. Metall. Mater. 50 (2005) 87–99.
[12] E.F. Rauch, M. Veron, Materialwiss. Werkstofftech. 36 (2005) 552–556.
[13] A.D. Darbal, K.J. Ganesh, X. Liu, S.B. Lee, J. Ledonne, T. Sun, B. Yao, A.P. Warren, G.S. Rohrer, A.D. Rollett, P.J. Ferreira, K.R. Coffey, K. Barmak, Microsc. Microanal. 19 (2013) 111–119.
[14] T. Sun, B. Yao, A.P. Warren, K. Barmak, M.F. Toney, R.E. Peale, K.R. Coffey, Phys. Rev. B 81 (155454) (2010) 1–12.
[15] D. Choi, B.C. Wang, S. Chung, X. Liu, A. Darbal, A. Wise, N.T. Nuhfer, K. Barmak, A.P. Warren, K.R. Coffey, M.F. Toney, J. Vac. Sci. Technol. A 29 (051512) (2011) 1–8.
[16] K.J. Ganesh, A.D. Darbal, S. Rajasekhara, G.S. Rohrer, K. Barmak, P.J. Ferreira, Nanotechnology 23 (135702) (2012) 1–7.
[17] D.M. Saylor, B.S. El-Dasher, B.L. Adams, G.S. Rohrer, Metall. Mater. Trans. A 35A (2004) 1981–1989.
[18] G.S. Rohrer, J. Am. Ceram. Soc. 94 (2011) 633–646.
[19] H. Beladi, G.S. Rohrer, Acta Mater. 61 (2013) 1404–1412.
[20] H. Beladi, G.S. Rohrer, Metall. Mater. Trans. A 44A (2013) 115–124.
[21] A. Morawiec, J. Appl. Crystallogr. 44 (2011) 1152–1156.
[22] G.S. Rohrer, J. Mater. Sci. 46 (2011) 5881–5895.
[23] K. Barmak, E. Eggeling, M. Emelianenko, Y. Ephshteyn, D. Kinderlehrer, R. Sharp, S. Ta'asan, Phys. Rev. B 83 (134117) (2011) 1–12.
[24] E.A. Holm, D.L. Olmsted, S.M. Foiles, Scr. Mater. 63 (2010) 905–908.
[25] E.A. Holm, G.S. Rohrer, S.M. Foiles, A.D. Rollett, H.M. Miller, D.L. Olmsted, Acta Mater. 59 (2011) 5250–5256.
[26] H.K. Kim, W.S. Ko, H.J. Lee, S.G. Kim, B.J. Lee, Scr. Mater. 64 (2011) 1152–1155.
[27] M.A. Tschopp, K.N. Solanki, F. Gao, X. Sun, M.A. Khaleel, M.F. Horstemeyer, Phys. Rev. B 85 (064108) (2012) 1–21.